

Neural Correlates of Vibrissa Resonance: Band-Pass and Somatotopic Representation of High-Frequency Stimuli

Mark L. Andermann,^{1,2,3} Jason Ritt,¹
Maria A. Neimark,² and Christopher I. Moore^{1,2,3,*}

¹McGovern Institute for Brain Research
Department of Brain and Cognitive Sciences
MIT

Cambridge, Massachusetts 02139

²Program in Biophysics

Harvard University

Cambridge, Massachusetts 02115

³Martinos Center

Massachusetts General Hospital

Charlestown, Massachusetts 02129

Summary

The array of vibrissae on a rat's face is the first stage of a high-resolution tactile sensing system. Recently, it was discovered that vibrissae (whiskers) resonate when stimulated at specific frequencies, generating several-fold increases in motion amplitude. We investigated the neural correlates of vibrissa resonance in trigeminal ganglion and primary somatosensory cortex (SI) neurons (regular and fast spiking units) by presenting low-amplitude, high-frequency vibrissa stimulation. We found that somatosensory neurons showed band-pass tuning and enhanced sensitivity to small amplitude stimuli, reflecting the resonance amplification of vibrissa motion. Further, a putative somatotopic map of frequency selectivity was observed in SI, with isofrequency columns extending along the representations of arcs of vibrissae, in agreement with the gradient in vibrissa resonance across the vibrissa pad. These findings suggest several parallels between frequency processing in the vibrissa system and the auditory system and have important implications for detection and discrimination of tactile information.

Introduction

The vibrissa sensory system of rats is capable of high-resolution tactile discrimination and has served as one of the key model systems for studying the organization of mammalian sensory processing (Woolsey and Van der Loos, 1970). We recently discovered a novel aspect of vibrissa biomechanics that may contribute to perception: vibrissae resonate when presented with a relatively narrow range of high-frequency stimuli, often amplifying input signals by an order of magnitude (Neimark et al., 2001, 2003; see also Hartmann et al., 2003). Further, the resonant frequencies vary as a function of length, with longer vibrissae displaying lower resonance frequencies. As such, the systematic progression of vibrissa lengths on the rat face, from long in the back to shorter in the front, creates an orderly facial map of frequency specificity (Neimark et al., 2003). The frequency-specific amplification provided by vibrissa resonance may en-

hance the detection and discrimination of high-frequency signals generated when vibrissae are swept over a surface texture (e.g., sandpaper; Neimark et al., 2003; Mehta and Kleinfeld, 2004; Moore, 2004). Rats show high acuity for these spatial frequency discriminations, and these tasks are known to depend on an intact primary somatosensory cortex (Carvell and Simons, 1990, 1995; Guic-Robles et al., 1989, 1992).

Vibrissa resonance has several potentially important neural coding implications. Neural transmission of vibrissa inputs begins in the peripheral input nerve, the trigeminal ganglion (NV), and is relayed somatotopically via the brainstem (Minnery and Simons, 2003) and thalamus (Diamond, 1995) to the primary somatosensory "barrel" cortex (SI) (Woolsey and Van der Loos, 1970). The organization of the vibrissa-to-barrel pathway leads to several predictions regarding neural responses to high-frequency stimuli presented to intact vibrissae. Two central predictions are (1) neurons in this pathway will demonstrate frequency tuning reflecting the resonance properties of their somatotopically associated vibrissa, and (2) the systematic map of frequency tuning across facial vibrissae is conferred to somatotopic neural maps.

To investigate these hypotheses, we recorded from NV and SI. We found that NV neurons and fast spiking (FSU) and regular spiking (RSU) neurons in SI showed distinct band-pass tuning, in agreement with vibrissa tuning. We also observed a somatotopic frequency map in SI, organized into "isofrequency columns" that were co-extensive with the barrel column representation of arcs of vibrissae. These findings suggest that the sensory transduction and neural processing of vibrotactile frequency information by vibrissae parallels the transduction and neural representation of sound stimuli in the auditory system (von Bekesy, 1947; Geisler, 1998). Preliminary reports of these data have been presented in abstract form (M.L. Andermann et al., 2002, 2003, Soc. Neurosci., abstract).

Results

Vibrissa Resonance

Figure 1 depicts a typical vibrissa frequency tuning curve. Tuning curves were generated by deflecting a vibrissa at its distal end with sinusoidal stimuli of constant amplitude across multiple frequencies (Figure 1B, inset). In this example, a ~7-fold increase in the amplitude of motion of the B2 vibrissa was seen at the fundamental resonance frequency (FRF) of the vibrissa (182 Hz; Figure 1B, ii). In contrast, motion amplitudes at lower (65 Hz; Figure 1B, i) and higher (230 Hz; Figure 1B, iii) frequencies were significantly smaller, providing band-pass amplification of vibrissa motion. The frequency tuning of vibrissae is inversely proportional to their length: longer, more posterior vibrissae demonstrate lower frequency tuning, while shorter, more anterior vibrissae demonstrate higher frequency tuning (Neimark et al., 2003). As such, a systematic "map" of frequency

*Correspondence: cim@ai.mit.edu

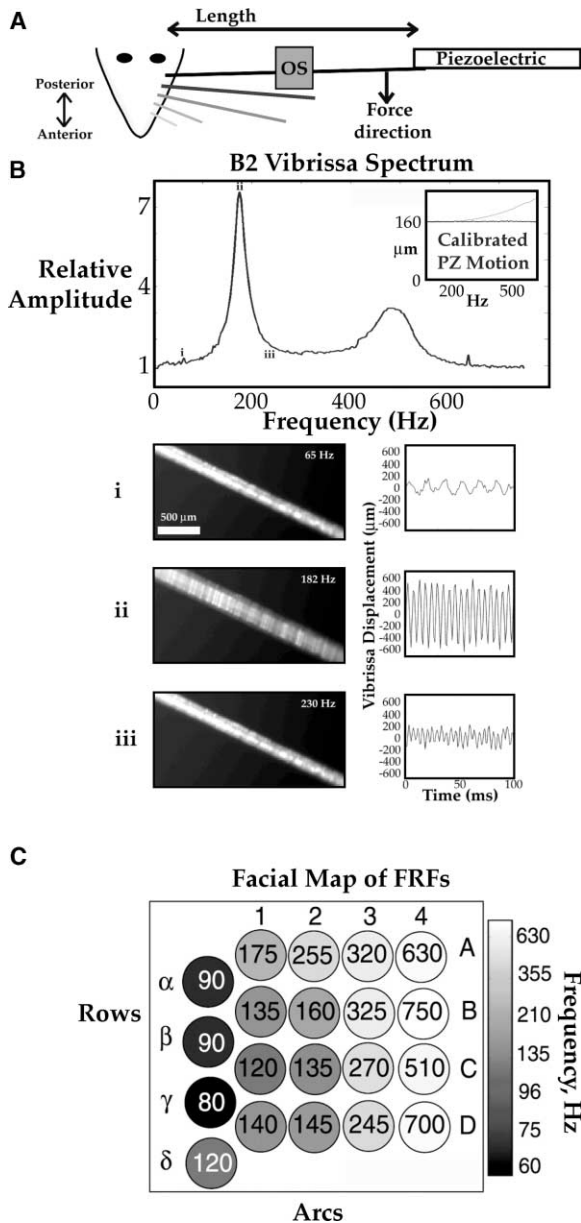


Figure 1. Example of Vibrissa Resonance

(A) During neural recording, an optical sensor (OS) monitored vibrissa motion driven at the vibrissa tip with a customized piezoelectric (PZ) stimulator.

(B) An example of vibrissa resonance. When a constant amplitude stimulus ($80\ \mu\text{m}$) was applied to the B2 vibrissa tip at frequencies from 5 to 750 Hz, a ~ 7 -fold increase in vibrissa motion was observed at 182 Hz, the vibrissa fundamental resonance frequency (FRF). Inset: frequency response of piezoelectric stimulator before (light gray) and after (dark gray) calibration. The specificity of this band-pass amplification can be appreciated in still photographs of the blur of vibrissa motion and in photodiode traces in (i), (ii), and (iii). These images show greater motion at the FRF than at frequencies below (65 Hz) and above (230 Hz).

(C) The length of a vibrissa is a key determinant in its resonance tuning, with longer vibrissae having lower FRFs. This relation creates a somatotopic map of FRF tuning across the rat face, with tuning from lower to higher frequencies across the same rat mystacial pad from posterior to anterior arcs of vibrissae (modified, with permission, from Neimark et al., 2003).

tuning is present in the resonance transduction properties of the vibrissae, with similar FRFs along each arc and a gradient in FRFs along each row (Figure 1C).

Response Properties of Trigeminal Ganglion and Cortical Neurons

To characterize the influence of vibrissa resonance on trigeminal (NV) or cortical (SI) evoked activity, we recorded single-unit action potential activity while applying constant amplitude sinusoidal stimuli to the distal end of the principal vibrissa (PV) for 500 ms at multiple frequencies (see Experimental Procedures). In SI, a dense sampling (steps ≤ 10 Hz) with a $160\ \mu\text{m}$ stimulus was conducted in a 200 Hz range surrounding the vibrissa FRF. Because of the higher signal to noise ratio, greater sensitivity, and greater stability of NV recordings, the NV experiments were broadened to include a 50–500 Hz range, and an $80\ \mu\text{m}$ stimulus was employed. Single-unit cortical recordings were made from the middle layers of SI (~ 500 – $950\ \mu\text{m}$; Figure 2A, top right) and were sorted into fast spiking units (FSUs, putative inhibitory interneurons) and regular spiking units (RSUs, putative excitatory) according to spike waveform shapes (Figure 2A; Bruno and Simons, 2002; Mountcastle et al., 1969; Swadlow, 2003).

Figure 2B shows the normalized peristimulus time histogram (PSTH) for NV and SI neurons, averaged across all experiments and frequencies within 100 Hz of the FRF. While the low-amplitude, high-frequency stimuli employed in this study evoked responses in both the periphery and SI, several differences existed among these response categories, as predicted by previous studies. First, NV neurons demonstrated profound sustained firing relative to onset responses. This sustained firing was less prominent in cortical responses (Arabzadeh et al., 2003; Zucker and Welker, 1969). The ratios of sustained mean firing (100–500 ms) to onset firing (0–100 ms) were .92, .34, and .37 for the NV, FSU, and RSU categories, respectively. Second, mean firing rates over the entire stimulus duration (500 ms) were significantly greater for FSU responses (9.91 ± 9.7 Hz, mean \pm SD; $n = 26$) than for RSU responses (1.38 ± 1.61 Hz, mean \pm SD; $n = 44$; $p = 0.00008$; two-tailed Student's *t* test; Simons and Carvell, 1989; Lee and Simons, 2003). Third, peripheral neurons showed the shortest onset latencies (9.7 ms), followed by FSU responses (13.2 ms) and RSU responses (15.8 ms; Figure 2B, bottom), consistent with fast, potent feed-forward inputs to FSUs in SI (Swadlow, 2003).

Frequency-Related Responses in NV

If a response was evoked for any frequency in the sampled range, NV neurons typically displayed frequency tuning. An example of this frequency relationship is shown for an NV unit driven by B2 vibrissa stimulation (Figure 3A). The frequency at which this neuron showed the largest amplitude response (the “best frequency” or BF; see Experimental Procedures) (180 Hz) was nearly identical to the FRF of the corresponding vibrissa (175 Hz) and, overall, the neural tuning curve (Figure 3A, top) closely matched vibrissa amplification (Figure 3A, middle). This frequency specificity in NV neurons was evident across a range of vibrissa FRFs (Figures 3B and

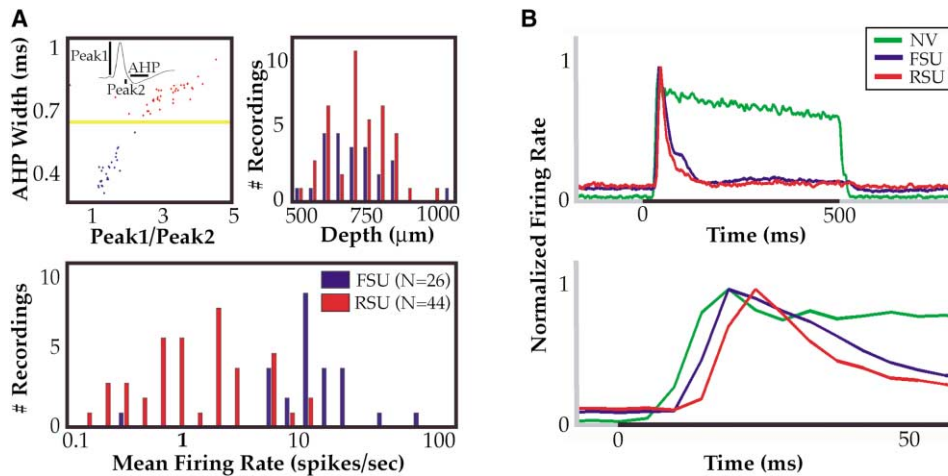


Figure 2. Classification of Neural Recordings

(A) Top left: isolated cortical single units were classified as fast spiking (FSU, blue) or regular spiking (RSU, red) based on the relative peak amplitudes and the width of the “after-hyperpolarization” (AHP) of the extracellular spike waveform. The inset shows a typical RSU spike demonstrating a longer AHP and less biphasic waveform (Peak1/Peak2–4). Top right: distribution of recording depths for FSUs and RSUs in SI. Bottom: histogram of average evoked firing rates for FSUs and RSUs across all stimulation frequencies.

(B) Top: normalized peristimulus response histograms (PSTH) across all recordings from single trigeminal ganglion neurons (NV; green) and SI FSUs (blue) and RSUs (red), averaged over all 500 ms high-frequency sinusoidal bursts. Bottom: expanded plots show increasing onset latencies from NV to FSU to RSU recordings.

3C). Not all NV units were driven by the small amplitude stimuli employed in this study: 17 of 29 responded to at least one of the frequencies within ± 100 Hz of the FRF during the period 25–100 ms after stimulus onset. This incidence is consistent with the wide range of known threshold firing amplitudes of NV neurons (Zucker and Welker, 1969). When a significant firing increase was recorded at any frequency, a BF was observed in 88% of cases ($n = 15/17$), and trigeminal BFs were well aligned with FRFs of vibrissa tuning curves. The absolute value of the frequency difference between BF and FRF values ($BF - FRF$) was 16.7 ± 3.5 Hz (mean \pm SE), and the mean difference between BF and FRF values across the sample ($BF - FRF$; 2.6 ± 6.5 Hz, mean \pm SE) was not significantly different from zero (two-tailed t test, $p = .34$).

Frequency-Related Responses in SI

Cortical responses also demonstrated high-frequency tuning that was consistently related to the corresponding vibrissa resonance. Paralleling the responses observed in NV neurons, RSU and FSU responses demonstrated several-fold increases in firing rate that were correlated with proximity to the FRF (Figure 3). Consistent with previous findings of high FSU sensitivity (Swadlow, 2003), a significant response was observed to at least one frequency of stimulation for all FSUs recorded for the period 25–100 ms poststimulus onset ($n = 26/26$), and frequency tuning (i.e., a BF) was observed in 81% of these cases ($n = 21/26$; Figure 3B). The absolute value of the frequency difference between the BF and FRF was greater for FSU than for NV recordings, 34.2 ± 5.1 Hz (mean \pm SE). This greater difference resulted from the trend for FSU BFs to be higher frequency than corresponding FRFs, as demonstrated in a shift of the mean BF value to 18.1 ± 9.2 Hz above the FRF (mean \pm

SE; two-tailed t test, $p = .07$; Figure 3C). The probability of significant RSU activity evoked by any frequency in the sample range was also high ($n = 37/44$), as was the likelihood of finding a BF (70%, $n = 26/37$). In contrast to FSU responses, however, RSUs demonstrated a broader dispersion of BFs around the FRF ($|BF - FRF|$; 35.0 ± 5.6 Hz, mean \pm SE) and, as with trigeminal responses, this distribution was not biased to higher or lower frequencies (Figures 3B and 3C; $BF - FRF$; 10.0 ± 9.2 Hz, mean \pm SE; two-tailed t test, $p = .29$).

Comparisons of Frequency Tuning across Neural Categories

To provide a direct visualization of the variance in neural tuning across individual recordings, the tuning curves for all responses in which significant activity could be evoked are shown in Figure 4A. Based on findings described in Supplemental Data (<http://www.neuron.org/cgi/content/full/42/3/451/DC1>), analyses were conducted for the interval 25–100 ms poststimulus onset, an interval in which vibrissa motion has reached its maximum resonant amplitude (Figure 6A) and in which neural activity has not attenuated in cortical PSTHs (Figure 2). For this epoch, we quantified the degree of neural frequency tuning with a commonly used metric, the quality factor “Q.” For evoked activity, “neural Q” was defined as the $BF/(\text{neural tuning bandwidth})$. Similarly, “vibrissa motion Q” was defined as the $FRF/(\text{motion tuning bandwidth}) = FRF/\omega$ (see Experimental Procedures). Tuning curves with higher Q values possess narrower bandwidths, and hence sharper tuning. The frequency tuning curves for NV and SI recordings were grouped for display purposes by this neural Q value, and central aspects of the data can be appreciated by this visualization. First, inspection of the vibrissa motion plots across all neural Q categories indicates that the sharpness of

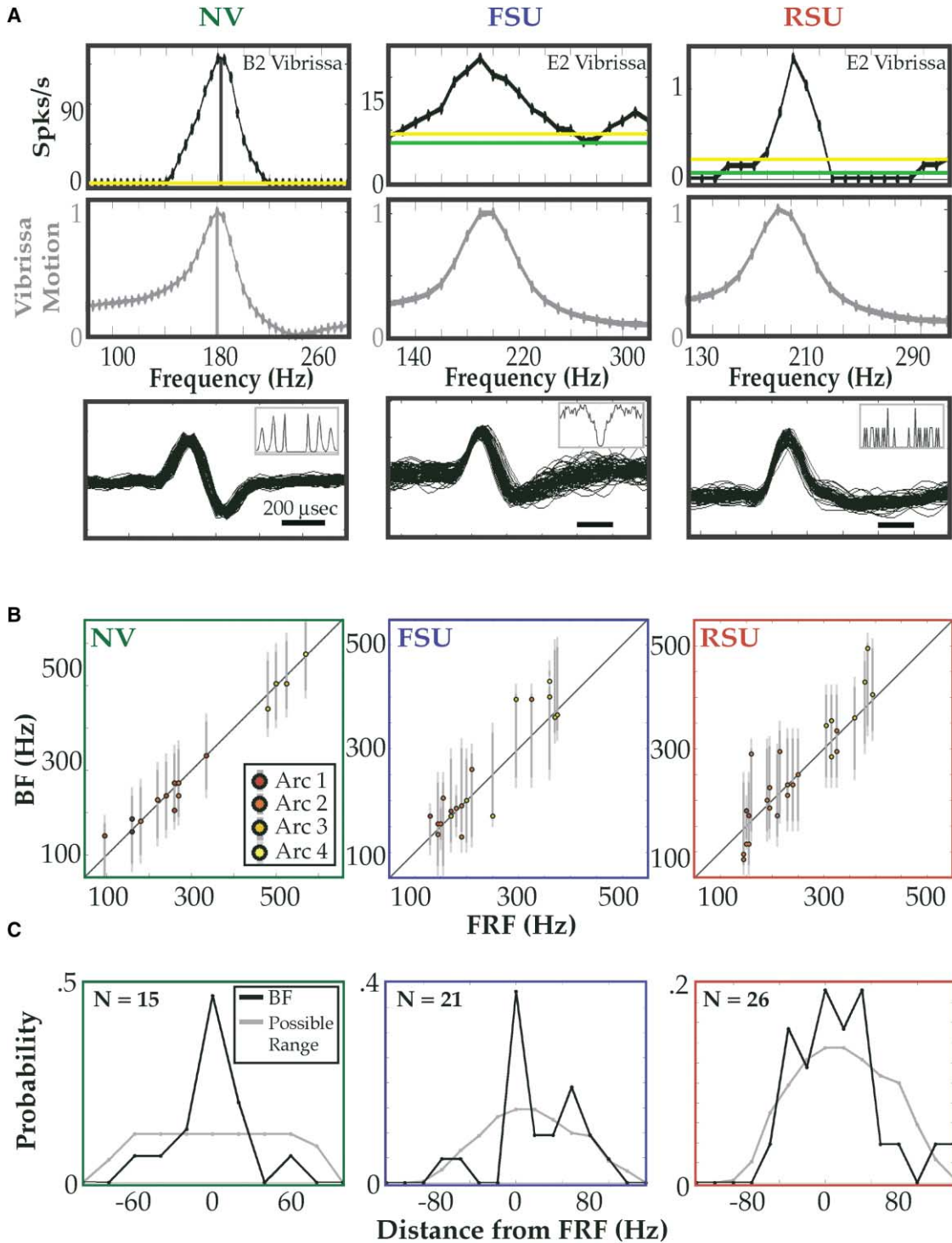


Figure 3. Neural Responses to Vibrissa Resonance

(A) Left: an example of a trigeminal ganglion (NV) single unit driven by B2 vibrissa stimulation at multiple frequencies. Spiking rate (top) shows a strong relation to vibrissa motion amplitude (middle). Vertical bars indicate the best frequency (BF, black), the frequency that drove peak neural activity, and the fundamental resonance frequency (FRF, gray), the frequency that drove peak vibrissa motion. Horizontal lines indicate prestimulus firing rate (green) and significant evoked firing rate threshold (yellow; see Experimental Procedures). Plots of 50 spike waveforms (bottom) and autocorrelograms (inset) confirmed the absence of spike contamination. Middle and right: example tuning curves for a cortical fast spiking unit (FSU) and a regular spiking unit (RSU). While both examples were obtained during the same penetration (FSU depth, 671 μ m; RSU depth, 559 μ m; E2 vibrissa stimulation), the neural tuning curve for the RSU is sharper than for the FSU, reflecting the overall trend in the data.

(B) The relation between BFs and FRFs for each neural category. Colors denote arc identity of stimulated vibrissae. Vertical bars indicate all applied frequencies (light gray) and the range from which a BF could have been defined (dark gray; see Experimental Procedures).

(C) The probability distribution of the difference between BF and FRF (BF - FRF, black) and the probability distribution of frequencies from which a BF could have been defined (gray). The gray distribution is nonuniform because of differences in sampling range relative to the FRF.

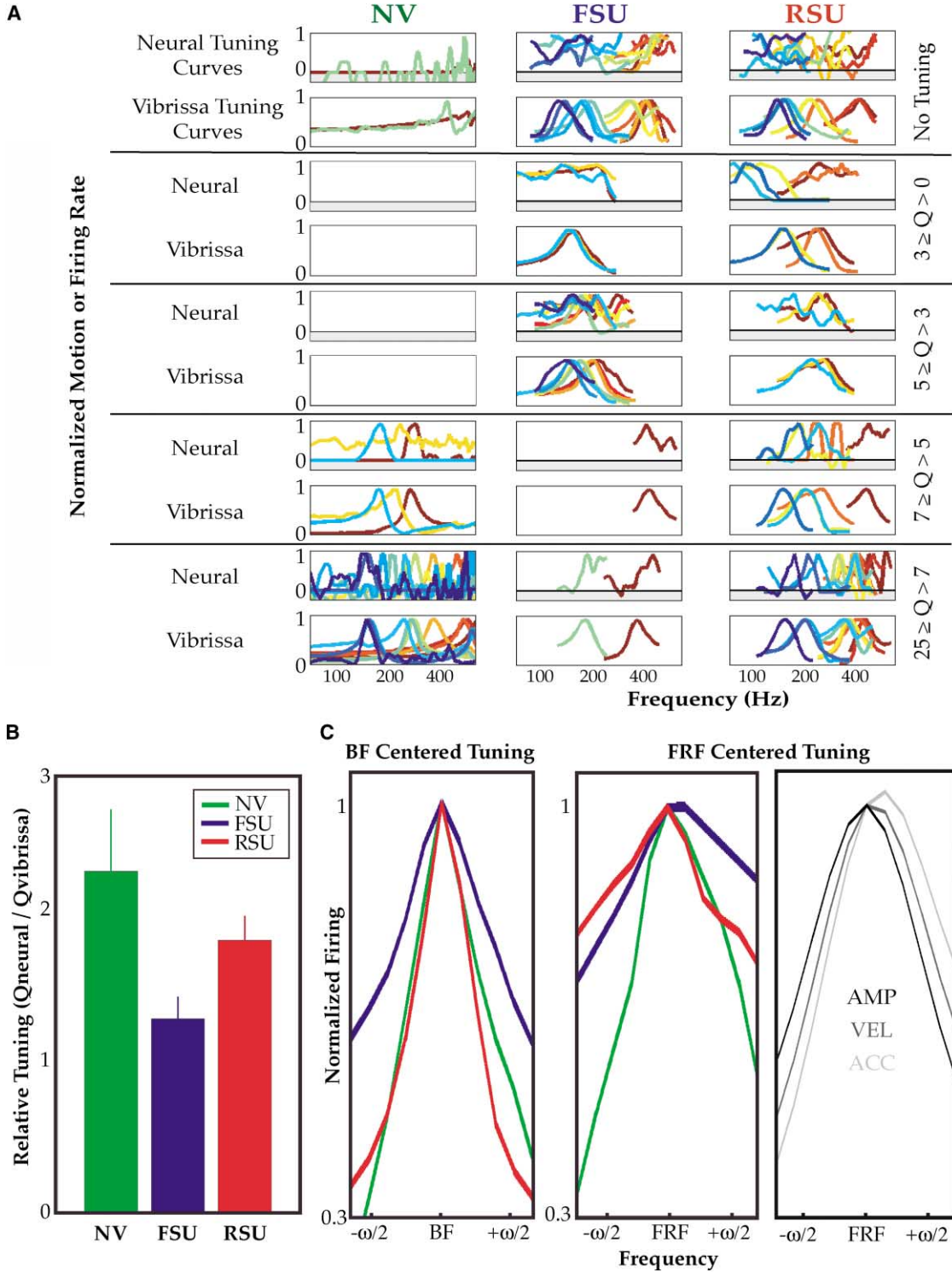


Figure 4. Neural Tuning Varies between Cell Types

(A) All frequency tuning curves with driven responses to at least one frequency are plotted (log-linear scale), classified within each neural category by the degree of tuning sharpness, neural Q (see Experimental Procedures). Neural tuning curves were plotted after subtracting prestimulus firing and then normalizing by peak evoked activity. Negative values indicate suppression of firing (shaded regions). Corresponding vibrissa motion tuning curves are plotted below each neural category for comparison. Nontuned cases ($Q = 0$) typically demonstrated low- or high-pass tuning. Vibrissa motion tuning sharpness was relatively constant across neural tuning categories.

(B) The relative degree of neural tuning across categories was calculated as $(\text{neural } Q)/(\text{vibrissa } Q)$ (mean \pm SE). Tuning was significantly sharper for NV and RSU response categories than for FSUs.

(C) Comparison of average BF- and FRF-centered tuning curves across neural categories. Tuning of driven RSUs in normalized BF-centered plots (left) was comparable to that of NV neurons. The FRF-centered, normalized tuning curves (middle) demonstrated tuning for all neural categories, despite jitter in BF relative to FRF for individual recordings (Figures 3B and 3C). Average FRF-centered vibrissa motion amplitude (black), peak velocity (dark gray), and peak acceleration (light gray) frequency tuning curves are plotted for comparison (right). The FRF-centered FSU tuning displayed a profile that appeared to match velocity/acceleration, while the NV and RSU tuning profiles best matched motion amplitude.

vibrissa frequency tuning was relatively constant, independent of neural tuning. Second, FSU recordings were distributed into higher plots in this display, indicating lower tuning as compared to RSU and NV recordings.

The basic qualitative trends in Figure 4A were reflected across the sample in the incidence and degree of tuning. A larger proportion of driven NV and RSU neurons showed band pass tuning (88% and 64%, respectively) as compared to FSUs (57%; see Supplemental Data at <http://www.neuron.org/cgi/content/full/42/3/451/DC1>). Further, tuning sharpness was higher for NV and RSU neurons than for FSUs, as demonstrated by the (neural Q)/(vibrissa motion Q) value, a ratio that normalizes differences in neural tuning by variations in vibrissa tuning between recordings (Figure 4B; ANOVA, $p = 0.0005$). The average NV tuning ratios demonstrated significantly sharper tuning than FSU ($p = 0.002$) responses, and RSUs were marginally more sharply tuned than FSUs ($p = .06$).

To compare tuning across neural categories, BF- and FRF-centered average tuning curves were constructed (Figure 4C, left and middle). These tuning curves were generated by centering individual tuning curves on the peak of neural tuning (BF) or of vibrissa tuning (FRF) and averaging across the sample (see Experimental Procedures). In the case of BF-centered plots, no assumption is made about the association between neural tuning and vibrissa tuning. In contrast, FRF-centered tuning curves make no assumption about frequency tuning of neural activity, and data were averaged across all experiments in which at least one stimulus frequency drove a significant response. If all neural responses were frequency tuned but had no association with vibrissa tuning (i.e., peak tuning values were equally distributed throughout the sampled frequencies), then a flat average activity level across frequencies would result from FRF-centered averaging. Both BF- and FRF-centered average tuning curves showed significant tuning for NV, FSU, and RSU responses, and significant differences were observed between neural categories (Figure 4C). As quantified in Figure 4B, BF-centered average tuning curves were sharper for NV and RSU responses than for FSU responses. The FRF-centered average tuning curves demonstrated that the net response from each neural category sampled was tuned around the vibrissa FRF. The higher-frequency bias observed in these plots for FSU responses may result from velocity and/or acceleration sensitivity (Figure 4C, right).

Spatial Localization of Frequency Preference within the Somatotopic Map

The systematic gradient of frequency-tuned responses across the rat face strongly suggests the existence of central frequency maps. Further, because vibrissae within an arc have similar resonance tuning, the peripheral resonance-derived map predicts that similar frequency responses should be observed in an arc of vibrissa, forming "isofrequency bands" across multiple vibrissa representation centers (Figure 5A). To investigate these predictions, the neural BF was plotted as a function of barrel column arc identity (Figure 5B), with vibrissae FRFs displayed for comparison. As expected from the close association of BF and FRF values (Figures

3B, 3C, and 4A), a frequency gradient in BF was observed for each neural category studied, with several hundred Hz differences between mean BFs in posterior and anterior arcs of barrel columns (see also pseudocolor arc identity of individual BFs in Figure 3B).

A complete assessment of whether the observed frequency map will persist during multiple-vibrissa stimulation is beyond the scope of this initial study. However, a preliminary example of simultaneous stimulation of β and C2 vibrissae with paired multiunit recordings in the β and C2 barrel columns in SI (~ 2 barrels apart) provides evidence for the spatial localization of resonance frequency tuning within the principal vibrissa barrel column (Figure 5C).

Spatial Localization of Latency within the Somatotopic Map

The intrinsic biomechanics of vibrissae also suggest a second kind of gradient/map is present within somatotopic vibrissa representations. Intact vibrissae are underdamped, and impulse-response measurements have shown large damping time constants ($\tau \sim 5\text{--}30$ ms; Neimark et al., 2001, 2003; Hartmann et al., 2003), such that vibrissa responses to sinusoidal burst stimulation at the FRF should show a gradual rise in amplitude. Because time constants for resonance evolution should vary proportionally with increasing vibrissa length, vibrissae in posterior arcs were hypothesized to drive longer latency poststimulus onset responses in corresponding SI neurons. In agreement with these predictions, the rise time of vibrissa motion at the FRF decreased as a function of arc number (for arcs 1–4, $\tau = 16.81 \pm 2.5$, 13.59 ± 0.47 , 8.93 ± 0.47 , 8.89 ± 0.52 ms, respectively; mean \pm SE; Figures 6A and 6B). This systematic distribution of vibrissa motion rise times across arcs was reflected in the neural onset latency from each arc, with shorter latencies in more anterior arcs of barrel columns for FSU and RSU responses (Figure 6B). In all four arcs, more rapid latencies were observed for FSU than for RSU responses (Figure 6), consistent with observed differences in the global average PSTHs (Figure 2B).

Discussion

We investigated neural responses in the periphery and cortex to high-frequency low-amplitude vibrissa stimuli. In contrast to most previous electrophysiological studies, in which vibrissa inputs were normalized by trimming (e.g., Armstrong-James and Fox, 1987; Moore and Nelson, 1998; Simons, 1985), the current study applied stimuli to untrimmed vibrissae, revealing a potentially important component of information processing in the vibrissa sensory system. In correspondence with the resonance frequency tuning observed under these conditions, the majority of responsive somatosensory neurons in the rat vibrissa-to-barrel pathway were frequency tuned. Further, the somatotopic organization of vibrissa tuning on the rat face resulted in a somatotopic gradient of frequency responsiveness across cortical neurons, providing evidence for a somatotopic frequency map and isofrequency columns in rat SI. Below, we discuss these results in the context of previous studies and consider their implications for detection and discrimination of

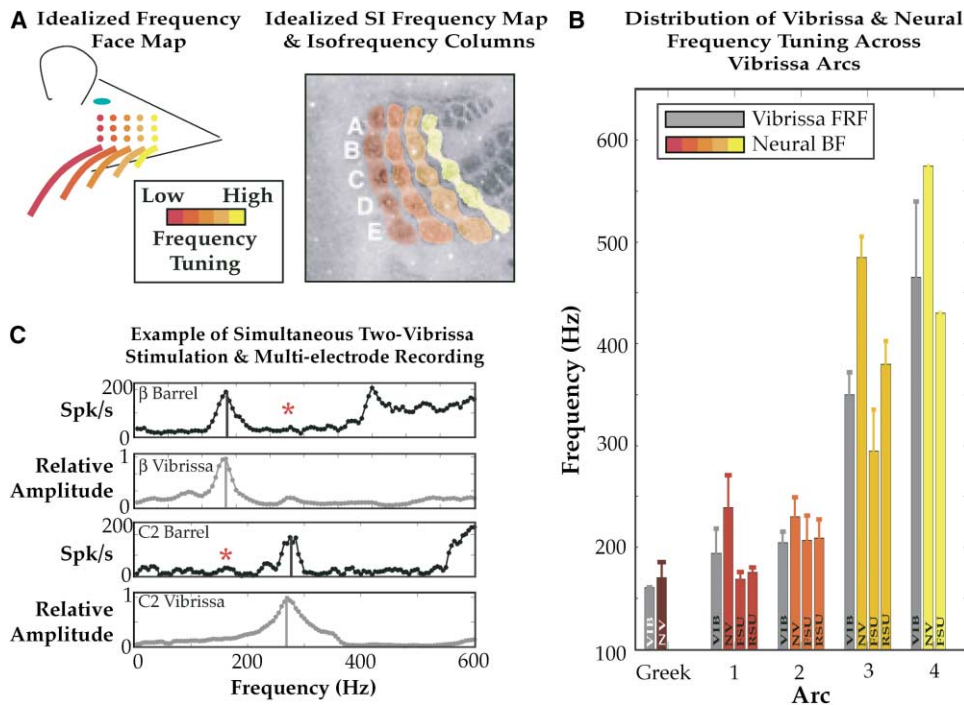


Figure 5. Somatotopic Organization of Frequency Tuning in SI

(A) Left: vibrissa lengths are similar along a vibrissa arc but vary along a vibrissa row, creating a systematic map of frequency tuning across the rat face, from low frequency-tuned vibrissae in posterior arcs to higher frequency-tuned vibrissae in anterior arcs (Neimark et al., 2003). Right: given the association between vibrissa length and FRF and between FRF and neural tuning, vibrissa resonance patterns predict a map of frequency tuning across SI, with isofrequency columns with similar frequency preferences extending along arcs of SI barrel columns (underlying anatomy from <http://www.neurobio.pitt.edu/barrels>).

(B) Within-arc averages of neural frequency tuning (BF; color scale) and vibrissa frequency tuning (FRF; gray) for all neural categories (mean \pm SE: vibrissa Ns for arcs from left to right, 2, 20, 62, 31, 3).

(C) A preliminary example of simultaneous multielectrode multiunit activity recordings (black traces) from the β and C2 barrel columns (~ 1 mm separation) and vibrissa monitoring (gray traces). When identical 80 μ m, 500 ms sinusoidal bursts were simultaneously applied to the β and C2 vibrissae, selective amplification of neural responses at the corresponding vibrissa FRF were observed, but not in response to the surround vibrissa (red asterisks).

high-frequency information. We then compare these findings with resonance-related frequency tuning in other sensory systems and discuss the limitations of this initial study.

Frequency-Specific Trigeminal Neuron Responses

In these experiments, trigeminal ganglion neurons (NV) showed distinct band-pass tuning that reflected vibrissa frequency tuning. This frequency specificity was evident in the examination of single neuron tuning curves (Figures 3A and 4A), in the distribution of neural Q values across the sample (Figures 4A and 4B), in the distribution of BFs (Figure 3B), and in averaged tuning curves centered on either the frequency that drove the peak vibrissa amplitude of motion (the fundamental resonance frequency, FRF) or centered on the frequency that drove the peak neural response (the best frequency, BF; Figure 4C). These findings show that, in the anesthetized animal, the intrinsic biomechanics of the vibrissa follicle do not impede the transduction into neural activity of resonant amplification. An essential further question is whether factors that are likely present in the behaving state, including increased tension of the muscles surrounding the vibrissa base and blood flow in the follicle,

could enhance or suppress the neural representation of vibrissa resonance (Yohro, 1977; Hartmann et al., 2003).

Previous studies have demonstrated acute sensitivity of NV neurons to the velocity of sensory input (Lichtenstein et al., 1990; Shoykhet et al., 2000). For a sinusoidal input, the velocity of the stimulus increases as the (amplitude) \times (frequency), and the acceleration as (amplitude) \times (frequency)². Thus, maximal velocity of vibrissa motion peaks at a higher frequency than does maximal amplitude of motion given a standard resonance amplification curve (Figure 4C). In accordance with the prediction of velocity sensitivity, NV neurons showed a bias in the shape of their BF-centered average tuning curves toward these higher frequencies (Figure 4C). This bias did not, however, shift the distribution of peak trigeminal tuning values (BF) to higher frequencies relative to the vibrissa FRF (Figure 3C): peak NV activity levels showed amplitude and not velocity tuning with respect to resonant vibrissa motion.

Previous studies have also shown that NV contains neurons with a variety of different response characteristics, including “rapidly adapting” (RA) and “slowly adapting” (SA) firing properties, as defined by ramp-and-hold stimuli (Lichtenstein et al., 1990). The trigeminal neurons recorded for this study were not character-

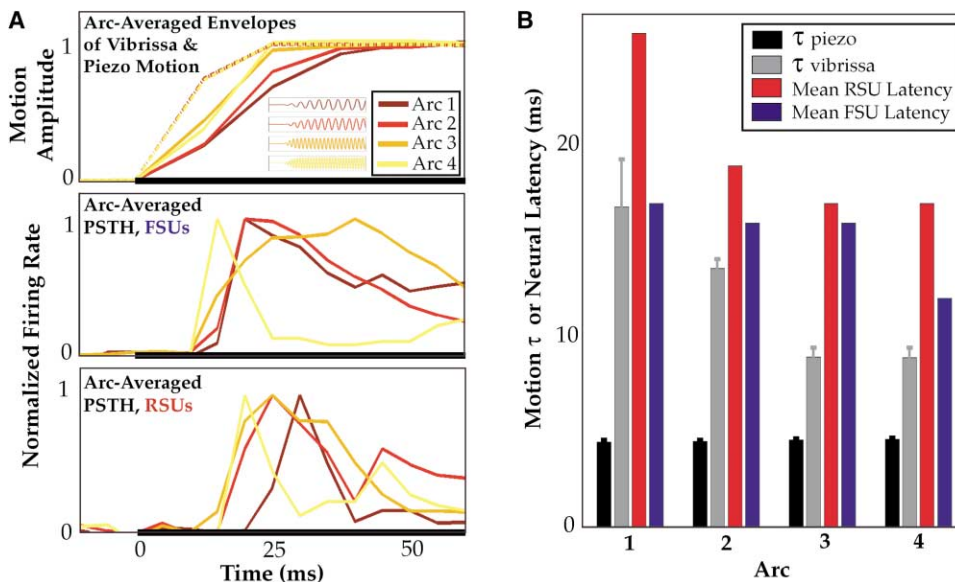


Figure 6. Somatotopic Organization of Latency in SI

(A) Average motion amplitude in each vibrissa arc (solid lines, top; arc 1 [red] to arc 4 [yellow]) evolved more slowly than piezoelectric stimulator motion envelopes (dashed lines; 12.5 ms sampling). Top, inset: examples of motion traces from vibrissae in arcs 1–4 during stimulation at the FRF showing the evolution of motion. A systematic gradient in latency to vibrissa motion amplification with increasing arc number was observed. This behavior was reflected in arc-averaged neural PSTHs for FSUs (middle) and RSUs (lower) for stimulation at frequencies near the FRF (± 10 Hz).

(B) These findings were quantified by fitting a single time constant (τ) exponential to piezo (black) and vibrissa (gray) motion envelopes (mean \pm SE). The latencies to 50% of peak response were calculated for the arc-averaged FSU (blue) and RSU (red) response PSTHs (Figure 6A). These data suggest that a latency gradient or “map” is present along rows of barrel columns in response to stimuli that drive vibrissa resonance.

ized with ramp-and-hold stimuli, but hand-mapping prior to recording suggested that, as in previous studies, the fraction of our NV sample that showed most sensitive responses were slowly adapting (Zucker and Welker, 1969) and that these neurons also showed sustained trains of neural activation to high-frequency stimuli (Gibson and Welker, 1983).

Frequency-Specific SI Neuron Responses

Both RSU and FSU cortical neurons demonstrated band-pass frequency tuning that reflected vibrissa frequency tuning. This tuning was evident in individual tuning curves (Figures 3A and 4A), in the distribution of neural Q values (Figures 4A and 4B), in the proximity of BFs to FRFs (Figures 3B and 3C), and in the FRF- and BF-centered averaged tuning curves (Figure 4C).

While tuning was observed for each neural category, response properties were not identical, as FSU and RSU activity differed in many respects. The FSU responses showed higher sensitivity to the small amplitude stimuli applied in this study, in agreement with previous studies (Simons and Carvell, 1989; Swadlow, 2003; see Supplemental Data at <http://www.neuron.org/cgi/content/full/42/3/451/DC1>). In accordance, FSU responses demonstrated relatively nonspecific frequency tuning, with relatively lower neural Q values (Figures 4A and 4B) and broader averaged FRF- and BF-centered tuning curves (Figure 4C) than RSU responses. This finding is also consistent with reports that FSUs show less-focused tuning for the spatial position of sensory input (Zhu and Connors, 1999) and for the angular direction of vibrissa

motion (Lee and Simons, 2003; Simons and Carvell, 1989). The FSU responses also revealed a strong bias toward higher frequency stimulation, as demonstrated by average tuning curves (Figure 4C) and the shift in the distribution of BF values toward higher frequencies (Figure 3C; Supplemental Data). These findings suggest that FSU responses were sensitive to the stimulus velocity and/or acceleration. This observation is in agreement with a variety of studies indicating that rat SI neurons, like trigeminal neurons, are differentially sensitive to velocity (Pinto et al., 2000), and with a recent study showing that the response of rat SI neurons to sinusoidal frequency-varying stimuli applied near the base of vibrissae demonstrated velocity sensitivity (Arabzadeh et al., 2003).

In contrast, RSU neurons demonstrated distinct firing properties. The RSUs showed significantly lower firing rates and a lower incidence of driven neurons. These putative excitatory neurons also showed sharper frequency tuning, as indicated by higher neural Q values (Figures 4A and 4B) and sharper average FRF- or BF-centered tuning curves (Figure 4C). The differences in neural tuning sharpness were independent of spontaneous firing rate, because all neural tuning curves (and Q values) were scaled from peak firing to prestimulus firing rates. Interestingly, despite sharper tuning of individual and FRF- or BF-averaged tuning curves, RSUs showed a broader distribution of BF values around the FRF as compared to FSU responses. This scatter in RSU BF values may reflect the sampling employed, as single amplitude stimuli and single direction stimuli were applied to RSUs: preliminary data (Andermann et al., 2002,

2003) suggest that the use of minimal amplitude tuning curves to determine the peak neural tuning generates significantly less scatter. Alternatively, when considered in the context of the sharper tuning of RSUs, the broader distribution of BFs could indicate that central mechanisms (see below) act to generate a local population of excitatory SI neurons that spans the range of frequencies surrounding the FRF with sharp frequency tuning when driven at higher amplitudes of vibrissa motion (e.g., 160 μm). This greater dispersion could allow for higher frequency resolution than is initially present in the distance between vibrissa resonance peaks.

Importantly, RSUs did not show the bias to higher frequencies observed in FSU frequency tuning curves. The lack of sensitivity of RSUs to increasing stimulation frequency may result from stronger inhibition at higher frequencies by FSUs, as a consequence of FSU sensitivity to higher frequency input (Figure 4C, Supplemental Data at <http://www.neuron.org/cgi/content/full/42/3/451/DC1>). Inhibitory sharpening of RSU frequency tuning is further suggested by decreased relative firing rates, often below prestimulus rates, of the most sharply tuned RSUs ($Q \geq 5$) at off-resonance frequencies (Figure 3A, right, and Figure 4A, bottom right). These data do not contradict the finding that RSU neurons are sensitive to the velocity of vibrissa deflection when stimuli are transiently applied with a nonresonating input (Lee and Simons, 2003; Pinto et al., 2000). The results do show that during the time epoch 25–100 ms after stimulus onset, an interval after vibrissa resonance has evolved and the time epoch demonstrating the highest incidence of SI frequency tuning, velocity tuning is not the defining characteristic of RSU responses. Further, these findings suggest that previous studies proposing the dominance of velocity cues in high-frequency responses of SI neurons (Arabzadeh et al., 2003) may have recorded predominantly multiunit and/or FSU activity, which closely parallel each other (see Supplemental Data).

The Spatial Organization of Neural Frequency Tuning in Rat SI

The vibrissa to barrel pathway is considered a canonical example of a spatial somatotopic map, with the receptive field properties of neurons in discrete modules throughout the ascending pathway reflecting the facial position of each vibrissa (Woolsey and Van der Loos, 1970). When stimuli identical to those employed here are applied, vibrissa resonance generates a distinct anterior-posterior map of frequency tuning on the face of the rat (Neimark et al., 2003). In agreement with this peripheral map, the somatotopic position of a cortical neural recording was a strong predictor of its frequency tuning. This relation between the peripheral map and cortical neural tuning is demonstrated by examination of individual FSU and RSU recordings with their underlying vibrissa receptive fields (Figures 3A and 4A) and by the relation of individual and averaged BF values with somatotopic position (Figures 3B and 5B). The similarity of FRFs along an arc of vibrissae predicts the existence of cortical isofrequency columns, groups of barrel columns, each representing a vibrissa arc, that is tuned to a narrow band of high-frequency signals. These findings suggest that two functional maps, one of position on

the face and one of frequency, overlap in the SI vibrissa representation. Further, the systematic shift across arcs in vibrissa amplification time constants and SI latencies (Figure 6B) suggests that a latency gradient is also present, similar to those observed in primary auditory cortex (Linden and Schreiner, 2003). While multiple representations of stimulus response features in overlapping cortical domains is a well-established organizing principle of the primary visual cortex (e.g., orientation and ocular dominance columns; LeVay et al., 1975), these findings present strong evidence for multiple overlapping maps across SI.

Much of the evidence provided here for a frequency map and isofrequency columns rests on the assumption that somatotopy can be extrapolated across our sample of rats, as data were accumulated across multiple animals, with any given animal contributing data from ≤ 3 vibrissae. This inference is reasonable, given the highly stereotyped somatotopic organization of the rat SI barrel cortex, as well as the finding of systematic increases in resonance frequency along each row in the same rat mystacial pad (Figure 1C; Neimark et al., 2003). The data presented here were also targeted to single vibrissa studies, leaving open the possibility that these map properties are not expressed during more complex stimulation patterns, for example when several vibrissae are stimulated simultaneously during palpation. While this question will require further investigation, the robust lateral inhibition observed in the SI vibrissa representation during repeated stimulation (Simons, 1985; Moore et al., 1999) suggests that the point spread of frequency-specific activity should sharpen during simultaneous multivibrissa contact, and initial findings provide evidence that map integrity is maintained across multiple vibrissa representations during the presentation of input to multiple vibrissae (Figure 5C and unpublished data).

Perceptual Implications of Frequency Tuning and a Frequency Map

Cortical neural frequency tuning and the putative SI frequency map may be useful in frequency discrimination. Rats show high acuity for roughness discrimination, a task that requires an intact SI cortex (Guic-Robles et al., 1992). For example, rats can use their vibrissae to discriminate between 1 mm and 1.06 mm gratings (Carvell and Simons, 1990, 1995). Typical whisking speeds over these textures (Bermejo et al., 1998; Carvell and Simons, 1995) should generate microvibrations of the vibrissa between ~ 100 and 1000 Hz, with only a $\sim 5\%$ difference in driving frequency between the two textures (Neimark et al., 2003). Rats could discriminate between these frequencies using a “place code,” comparing mean firing rates between isofrequency columns, with greater posterior map activity indicating lower-frequency driving signals (from lower spatial frequency textures) and vice versa. We emphasize that these relative judgments would not require that the rat “know” the temporal frequency generated by a given velocity convolved with a spatial frequency (a difficult decoding problem for a variety of reasons, including continued vibrissa growth). Rather, the perceiving animal would need to determine only the difference in signal strength along a posterior-anterior gradient.

During the course of rostral-caudal “whisking motions” across a surface, vibrissae within an arc likely exhibit pronounced synchrony in object contact (Sachdev et al., 2001), which may selectively increase response efficacy in a local band of same-arc SI cortical columns (Ahissar and Arieli, 2001; Ghazanfar and Nicolelis, 1997; Shimegi et al., 1999). Coding of similar frequency information across an arc could also increase robustness of resonance-related frequency coding, by attenuating the effects of loss or damage to any single vibrissa or the presence of a guard hair that could impede or modify resonance amplification. The integration of information along an isofrequency column could also enhance the separability of somatotopic and frequency-related information, helping to disambiguate the similar but not identical organization of these overlapping maps. The temporal evolution of vibrissa resonance could also facilitate frequency processing in at least two ways. First, the relative latency shift in the onset of activity in different arcs of vibrissae (Figure 6) could further distinguish the arc-specific integration of information. Second, the shortest latency responses within a barrel (e.g., 0–25 ms) could indicate the position of contact to the perceiving animal, while activity occurring at a longer latency (e.g., 25–100 ms) could indicate the frequency of input.

Neural Response Amplification

Amplification of the size of the neural response, resulting from the amplification of vibrissa motion, is a potentially crucial implication of vibrissa resonance. Rats are able to detect the presence of fine textures (e.g., 30 μm grooves spaced at 90 μm intervals; Carvell and Simons, 1990). While the nature of vibrissa transduction of such a surface during perception is not well understood, 30 μm vibrissa displacements, administered under the current protocol, would not have driven neural activation in the majority of our NV and SI recordings without accompanying vibrissa resonance (Neimark et al., 2003). If this contact occurred along the shaft of a vibrissa (e.g., at the midpoint), the relative amplitude would be equivalent to ~ 60 μm stimulation at the tip, a stimulus amplitude that was often unable to drive responses in our sample in the absence of resonance amplification. Even for the largest amplitude stimuli employed in this study (160 μm tip deflections), the presence of vibrissa resonance amplification was often required to evoke a significant response from SI neurons (Figures 3A, RSU example, and 4A). Neural signal amplification as a result of vibrissa resonance could facilitate the detection of fine textured stimuli that will generate high-frequency vibrissa vibrations (Neimark et al., 2003), potentially through a slip-stick interaction between the surface and vibrissa (Neimark et al., 2003; Mehta and Kleinfeld, 2004) and, more generally, of small amplitude vibrations in whatever way they are transmitted (e.g., through air).

Similarity to Other Sensory Systems

Resonance-related frequency tuning is found in a variety of sensory systems that function in various conduction media (solid surfaces, water, wind) and contribute to different sensory modalities (sound and touch stimuli). High-frequency water motions drive resonance in the

fish lateral line cupula (~ 380 Hz; van Netten and Khanna, 1993) and are also thought to play a role in vibrissa-based navigation in seals (Dehnhardt et al., 2001). Cockroach and cricket cercal hairs resonate in response to high-frequency wind stimuli, a potentially important indicator of oncoming predators (Plummer and Camhi, 1981; Roddey and Jacobs, 1996). Consistent with our findings for rat vibrissae, cricket cercal hairs demonstrate resonance frequencies that increase with decreasing hair length (~ 80 –500 Hz; Kondoh et al., 1991; Shimozawa and Kanou, 1984), and cricket cercal hair resonance is believed to underlie the neural high-frequency tuning observed in the spiking activity of various filiform receptor neurons (Roddey and Jacobs, 1996).

Vibrissa resonance and its neural correlates perhaps most closely parallel the organization of the auditory system. In the auditory pathway, resonance behavior in the cochlea translates sound pressure waves into tuned auditory receptive fields and a spatial map of frequency sensitivity (Geisler, 1998). The spatial mapping of tonotopy in the primary auditory cortex (AI) is organized in elongated horizontal isofrequency columns that follow a gradient of preferred frequencies (Abeles and Goldstein, 1970; Merzenich and Brugge, 1973). The putative frequency and latency maps and isofrequency columns across SI directly parallel this AI organization. These functional similarities between resonance frequency tuning in the vibrissa-to-barrel pathway and in auditory and other sensory systems suggest a convergent evolutionary solution to the representation of frequency-varying stimuli.

Future Directions and Limitations of the Present Study

The present study is an initial investigation of the neural correlates of vibrissa resonance. As such, several important domains have not been investigated, and there are limitations to the current data set. The present data provide almost no insight into the impact of higher resonance modes on neural activity. We chose not to focus the present report on these phenomena for several technical reasons and because the fundamental mode should provide the largest relative amplification (Landau and Lifshitz, 1975). Although higher harmonic resonance modes were not consistently observed in our data, they were observed in a limited number of recordings and can provide significant and potentially perceptually relevant amplification of vibrissa motion (see Figure 1A; Neimark et al., 2003; Hartmann et al., 2003; Mehta and Kleinfeld, 2004). Another important domain for further study is the relation between high-frequency resonance activity and the fine timing of spiking in the vibrissa sensory system (see autocorrelogram, Figure 3A, left; Deschenes et al., 2003; Gottschaldt and Vahle-Hinz, 1981). In this regard, the robust high-frequency oscillations that Barth and colleagues have observed in rat barrel cortex following transient vibrissa deflections (e.g., Jones et al., 2000) could interact with high frequency input driven at vibrissa resonance. Consistent with this hypothesis, preliminary studies suggest that an SI map of field potential peak frequency exists in the 400–600 Hz band (R.P. Dansereau et al., 2003, Soc. Neurosci., abstract).

Perhaps the most important limitation of the present

data set was the use of immobilized, anesthetized animals. While many advances in understanding the relation between sensory transduction and neural encoding at the peripheral and cortical levels have been made under similar conditions, the utility of the resonance-related response properties observed here cannot be specifically addressed without vibrissa monitoring and neural recording in awake and behaving animals.

Experimental Procedures

Surgery

All experiments were performed in compliance with research protocols approved by the Massachusetts General Hospital and Massachusetts Institute of Technology. Male Sprague-Dawley rats ($n = 24$; wt, mean \pm SD: 313 ± 85 g) were anesthetized with urethane (1.2 g/kg i.p. initial dose), and supplemental doses (10% of initial dose) were administered to maintain areflexive hindpaw-pinch response and steady EKG and respiration rate (90–120 breaths per min; Armstrong-James and Fox, 1987). Body temperature was maintained at 37°C using a servo-controlled heating blanket. The rat was held in a stereotaxic frame on a floating table to minimize external vibrations. A craniotomy and durotomy were performed, with a retaining well filled with warm mineral oil or saline. Following experiment termination, the rat was euthanized by urethane overdose (3 g/kg) and in a subset of cases perfused for cytochrome oxidase histology.

Electrophysiology

Parylene-coated tungsten microelectrodes (FHC or A-M Systems) with 2–10 M Ω impedance at 1 kHz were used for single-unit recording in the trigeminal ganglion (NV) and SI. Recordings from NV were conducted ipsilateral to vibrissa stimulation (6 mm anterior to Lambda, 2 mm lateral, \sim 10 mm ventral to the cortical surface; Shoykhet et al., 2000). Recordings from SI were conducted contralateral to vibrissa stimulation (1–4 mm posterior to Bregma, 4–7 mm lateral), \sim 500–950 μ m deep to the cortical surface, targeting layers III and IV as judged by micromanipulator readings and negative polarity of local field potential activity (Figure 2A, top right). These depths were confirmed by histological reconstruction of electrolytic lesions (\sim 18 μ A for 3 s) from 6 penetrations in 2 rats. Recordings were filtered (250/300–5000 Hz; Neurotrack and Neuralynx recording systems), amplified (5000 \times), digitized at 20,000 Hz or 33,657 Hz (cortical single unit recordings), and stored with stimulus markers. To isolate single units, recordings were further filtered (800–5000 Hz), and acceptable “multiunit” (MUA) waveforms (1.5 ms) containing voltage fluctuations exceeding ± 4 SD above prestimulus activity (0.5 ms minimal dead-time between events) were saved for spike clustering using custom-written software (MATLAB). Manually selected separable clusters of points in multiple scatter plots displaying maximal and minimal waveform amplitudes, and slopes were then subjected to additional criteria: (1) the autocorrelation function did not contain spike contamination within (-1 ms, 1 ms), and (2) firing was stable over the duration of recording. Stability was estimated by averaging the evoked response to successive 100 trial epochs and requiring that $\geq 70\%$ of these epochs were within 50% of the median epoch firing rate.

Vibrissa Stimulation

We employed custom-designed high-performance piezoelectric bimorphs (Piezo Systems, Inc., Q234-H4CL-303X) with a high fundamental resonance frequency (≥ 800 Hz, achieved by reducing piezoelectric length and attaching a 20 mm light wooden extension), calibrated with optoelectronics and compensating voltage adjustments to $< 3\%$ amplitude deviations and constant latencies for 500 ms sinusoidal stimulus bursts from 0 to 750 Hz (30–700 Hz for cortical single unit studies; see Figure 1B, inset, and Figure 6A, top, dashed lines). Voltage commands were generated in MATLAB, sent through an I/O board (NI), amplified (Thorlabs or Sensor Technologies), and sent to the piezoelectric. Sinusoidal stimuli were tapered at both ends using a sine function ($\sin(2^*\pi*t/40)$, t in [0 ms, 10 ms]) to minimize edge effects and frequency contamination.

The principle vibrissa (PV) was determined for a given site by hand-mapping individual vibrissae. The stimulator was then rigidly attached parallel to the long axis of the vibrissa at 1–2 mm from the untrimmed vibrissa tip using bone wax. Deflections were typically made in the preferred direction of angular vibrissa deflection for NV recordings and along the rostro-caudal axis for SI recordings. Rostro-caudal stimulation was used because cortical angular tuning curves are typically broader and the optimal direction is often difficult to estimate by manual deflection.

Vibrissa Monitoring

To measure vibrissa motion, an infrared slotted optical switch (< 10 μ m resolution; QVA series; Fairchild) with nearly linear responses to small (< 3 mm) static changes in position was placed at the estimated halfway point along the vibrissa length. In a subset of vibrissae from the posterior arcs, the relative tension on the vibrissa was adjusted as needed to optimize imaging of resonance peaks by increasing the amplitude of vibrissa motion. This modification in some cases increased the resonant frequency by ≤ 50 Hz. Motion signals were high-pass filtered above 10 Hz, amplified (100 \times), and digitized at 20,000 Hz or 33,657 Hz. To estimate relative vibrissa motion, a sinusoid at each driving frequency was convolved with the vibrissa motion signal over set epochs (0–25, 25–50, 50–100, 100–500, 25–100, or 0–500 ms after stimulus onset, see Supplemental Data at <http://www.neuron.org/cgi/content/full/42/3/451/DC1>), and the motion amplitude was calculated as the difference between minimal and maximal values of this convolution, followed by subtraction of the same measure over an equal duration prestimulus.

Stimulus Protocols and Tuning Curves

To obtain vibrissa amplitude and neural response frequency tuning curves, a sinusoidal stimulus was presented. For NV recordings, vibrissae were stimulated at 1 s intervals with 500 ms, 80 μ m sinusoidal bursts (≥ 3 trials/stimulus type) from 5 to 600 Hz at 5 Hz increments in randomized order ($n = 29$). Cortical single-unit recordings typically showed stronger adaptation to short interburst intervals, a shorter total recording window in which single-unit isolation could be maintained, and lower overall sensitivity to vibrissa motion, i.e., a larger tip stimulation was required to drive a significant response. Thus, for cortical recordings, vibrissae were presented with single-frequency bursts at 1 s (FSU, $n = 13$; RSU, $n = 31$) or 2 s (FSU, $n = 7$; RSU, $n = 19$) interburst intervals in randomized order with 500 ms, 160 μ m sinusoidal bursts (≥ 15 trials/stimulus type). Frequencies were sampled at 5 Hz ($n = 12$) or 10 Hz ($n = 58$) increments over 15 or 21 frequencies surrounding the vibrissa fundamental resonance frequency. Neural frequency tuning curves were defined as the average firing rate in a chosen interval after stimulus onset across stimulus frequencies. Similarly, to generate vibrissa frequency tuning curves, vibrissa motion amplitudes over the same period following stimulus onset were normalized to the amplitude at the fundamental resonance frequency (see below). The neural and vibrissa frequency tuning curves were smoothed using a 3-point boxcar filter, which minimized spurious peaks and was significantly smaller than the neural or vibrissa frequency tuning bandwidths in all cases.

We estimated the fundamental resonance frequency (FRF) for vibrissa motion and best frequency (BF) for neural response tuning curves. To identify the FRF, successively higher frequencies were evaluated, starting at 70 Hz (NV) or at the lowest frequency sampled (SI), and the FRF was defined as the frequency of greatest vibrissa motion amplitude that also displayed smaller amplification at frequencies in a 20 Hz window on either side. A well-defined FRF was found for $> 90\%$ of tested vibrissae. The neural BF was chosen as the frequency that evoked the largest response, at least 2 standard deviations above the mean firing rate calculated in an equal period prestimulus onset. Responses observed within 20 Hz of the edge of the sampled frequency range were excluded from BF consideration. Average neural tuning curves across the sample were then calculated, centered on either the FRF or BF. For inclusion in this analysis, the following criteria were applied to each recording. First, a neural BF had to exist, so that responses could be centered on the BF. Second, a minimal number of frequencies surrounding the FRF had to have been sampled (greater than or equal to ± 0.75 bandwidths of the vibrissa amplitude tuning curve), so that a full tuning curve

could be plotted. Third, for FRF-centered average tuning curves, a minimal level of neural activation existed for at least one frequency in a 100 Hz region surrounding the FRF, ≥ 2 SD above baseline firing rate in an equal time-period prestimulus: for NV recordings, we also required evoked responses >3 spikes/s (Brosch and Schreiner, 1999). For FRF-centered average tuning curves, the individual spike rate measures were averaged at each sampling interval, and this average neuronal response to resonant vibrissa stimulation was subsequently normalized to its value at the FRF. For BF-centered average tuning curves, individual responses were normalized to the BF and averaged.

Peak Frequencies and Degree of Tuning

We employed several metrics common to studies of auditory frequency tuning to characterize vibrissa and neural activity (Geisler, 1998). To measure the sharpness of vibrissa motion tuning curves, we defined a tuning bandwidth (ω) as the width of the curve at an intensity of 29% (3 dB) below the amplitude at the FRF (Oshinsky and Hoy, 2002). The vibrissa motion Q factor was then defined as the FRF divided by the motion tuning bandwidth (FRF/ ω). In a similar fashion, the neural tuning bandwidth was obtained by (1) subtracting baseline firing rates from the neural tuning curves and (2) calculating width of the resulting curve at 29% below peak firing. When a neural BF and neural frequency tuning bandwidth existed for the neural tuning curve, the neural Q factor was calculated as the BF divided by the neural bandwidth. Bandwidth edges were estimated using linear interpolation of points above and below the -3 dB line.

Acknowledgments

We thank David Boas, Cheryl Cheney, Amy Fisher, Catherine Garabedian, Stephanie Jones, Aimee Nelson, Andy Siegel, and Istvan Ulbert for technical assistance and helpful discussion. This work was supported by NSF (0316933) and NIH (1-RO1-NS045130-01). M.L.A. and M.A.N. are Howard Hughes Medical Institute Predoctoral fellows.

Received: June 6, 2003
Revised: February 24, 2004
Accepted: March 18, 2004
Published: May 12, 2004

References

Abeles, M., and Goldstein, M.H., Jr. (1970). Functional architecture in cat primary auditory cortex: columnar organization and organization according to depth. *J. Neurophysiol.* **33**, 172–187.

Ahissar, E., and Arieli, A. (2001). Figuring space by time. *Neuron* **32**, 185–201.

Arabzadeh, E., Petersen, R.S., and Diamond, M.E. (2003). Encoding of whisker vibration by rat barrel cortex neurons: implications for texture discrimination. *J. Neurosci.* **23**, 9146–9154.

Armstrong-James, M., and Fox, K. (1987). Spatiotemporal convergence and divergence in the rat S1 “barrel” cortex. *J. Comp. Neurol.* **263**, 265–281.

Bermejo, R., Houben, D., and Zeigler, H.P. (1998). Optoelectronic monitoring of individual whisker movements in rats. *J. Neurosci. Methods* **83**, 89–96.

Brosch, M., and Schreiner, C.E. (1999). Correlations between neural discharges are related to receptive field properties in cat primary auditory cortex. *Eur. J. Neurosci.* **11**, 3517–3530.

Bruno, R.M., and Simons, D.J. (2002). Feedforward mechanisms of excitatory and inhibitory cortical receptive fields. *J. Neurosci.* **22**, 10966–10975.

Carvell, G.E., and Simons, D.J. (1990). Biometric analyses of vibrissal tactile discrimination in the rat. *J. Neurosci.* **10**, 2638–2648.

Carvell, G.E., and Simons, D.J. (1995). Task- and subject-related differences in sensorimotor behavior during active touch. *Somatosens. Mot. Res.* **12**, 1–9.

Dehnhardt, G., Mauck, B., Hanke, W., and Bleckmann, H. (2001).

Hydrodynamic trail-following in harbor seals (*Phoca vitulina*). *Science* **293**, 102–104.

Deschenes, M., Timofeeva, E., and Lavalley, P. (2003). The relay of high-frequency sensory signals in the whisker-to-barreloid pathway. *J. Neurosci.* **23**, 6778–6787.

Diamond, M.E. (1995). *Somatosensory Thalamus of the Rat*, volume 11 (New York: Plenum Press).

Geisler, C. (1998). *From Sound to Synapse* (New York: Oxford University Press).

Ghazanfar, A.A., and Nicolelis, M.A. (1997). Nonlinear processing of tactile information in the thalamocortical loop. *J. Neurophysiol.* **78**, 506–510.

Gibson, J.M., and Welker, W.I. (1983). Quantitative studies of stimulus coding in first-order vibrissa afferents of rats. 2. Adaptation and coding of stimulus parameters. *Somatosens. Res.* **1**, 95–117.

Gottschaldt, K.M., and Vahle-Hinz, C. (1981). Merkel cell receptors: structure and transducer function. *Science* **214**, 183–186.

Guic-Robles, E., Valdivieso, C., and Guajardo, G. (1989). Rats can learn a roughness discrimination using only their vibrissal system. *Behav. Brain Res.* **37**, 285–289.

Guic-Robles, E., Jenkins, W.M., and Bravo, H. (1992). Vibrissal roughness discrimination is barrel cortex-dependent. *Behav. Brain Res.* **48**, 145–152.

Hartmann, M.J., Johnson, N.J., Towal, R.B., and Assad, C. (2003). Mechanical characteristics of rat vibrissae: resonant frequencies and damping in isolated whiskers and in the awake behaving animal. *J. Neurosci.* **23**, 6510–6519.

Jones, M.S., MacDonald, K.D., Choi, B., Dudek, F.E., and Barth, D.S. (2000). Intracellular correlates of fast (>200 Hz) electrical oscillations in rat somatosensory cortex. *J. Neurophysiol.* **84**, 1505–1518.

Kondoh, Y., Arima, T., Okuma, J., and Hasegawa, Y. (1991). Filter characteristics of cercal afferents in the cockroach. *J. Comp. Physiol. [A]* **169**, 653–662.

Landau, L., and Lifshitz, E. (1975). *Theory of Elasticity*, Volume 9 (Oxford: Pergamon Press).

Lee, S.H., and Simons, D.J. (2003). Angular tuning and velocity sensitivity in different neuron classes within layer 4 of rat barrel cortex. *J. Neurophysiol.* **91**, 223–229.

LeVay, S., Hubel, D.H., and Wiesel, T.N. (1975). The pattern of ocular dominance columns in macaque visual cortex revealed by a reduced silver stain. *J. Comp. Neurol.* **159**, 559–576.

Lichtenstein, S.H., Carvell, G.E., and Simons, D.J. (1990). Responses of rat trigeminal ganglion neurons to movements of vibrissae in different directions. *Somatosens. Mot. Res.* **7**, 47–65.

Linden, J.F., and Schreiner, C.E. (2003). Columnar transformations in auditory cortex? A comparison to visual and somatosensory cortices. *Cereb. Cortex* **13**, 83–89.

Mehta, S., and Kleinfeld, D. (2004). Frisking the whiskers: patterned sensory input in the rat vibrissa system. *Neuron* **41**, 181–184.

Merzenich, M.M., and Brugge, J.F. (1973). Representation of the cochlear partition of the superior temporal plane of the macaque monkey. *Brain Res.* **50**, 275–296.

Minnery, B.S., and Simons, D.J. (2003). Response properties of whisker-associated trigeminothalamic neurons in rat nucleus principalis. *J. Neurophysiol.* **89**, 40–56.

Moore, C.I. (2004). Frequency-dependent information processing in the vibrissa sensory system. *J. Neurophysiol.* **91**, 2390–2399.

Moore, C.I., and Nelson, S.B. (1998). Spatio-temporal subthreshold receptive fields in the vibrissa representation of rat primary somatosensory cortex. *J. Neurophysiol.* **80**, 2882–2892.

Moore, C.I., Nelson, S.B., and Sur, M. (1999). Dynamics of neural processing in rat somatosensory cortex. *Trends Neurosci.* **22**, 513–520.

Mountcastle, V.B., Talbot, W.H., Sakata, H., and Hyvarinen, J. (1969). Cortical neuronal mechanisms in flutter-vibration studied in unanesthetized monkeys. Neuronal periodicity and frequency discrimination. *J. Neurophysiol.* **32**, 452–484.

Neimark, M.A., Anderman, M.A., Hopfield, J.J., and Moore, C.I.

- (2001). A mechanical model of vibrissae as filters of textural information. Paper presented at Barrels XIV (Carlsbad, CA).
- Neimark, M.A., Andermann, M.L., Hopfield, J.J., and Moore, C.I. (2003). Vibrissa resonance as a transduction mechanism for tactile encoding. *J. Neurosci.* *23*, 6499–6509.
- Oshinsky, M.L., and Hoy, R.R. (2002). Physiology of the auditory afferents in an acoustic parasitoid fly. *J. Neurosci.* *22*, 7254–7263.
- Pinto, D.J., Brumberg, J.C., and Simons, D.J. (2000). Circuit dynamics and coding strategies in rodent somatosensory cortex. *J. Neurophysiol.* *83*, 1158–1166.
- Plummer, M.R., and Camhi, J.M. (1981). Discrimination of sensory signals from noise in the escape system of the cockroach: the role of wind acceleration. *J. Comp. Physiol.* *142*, 347–357.
- Roddey, J.C., and Jacobs, G.A. (1996). Information theoretic analysis of dynamical encoding by filiform mechanoreceptors in the cricket cercal system. *J. Neurophysiol.* *75*, 1365–1376.
- Sachdev, R.N., Sellien, H., and Ebner, F. (2001). Temporal organization of multi-whisker contact in rats. *Somatosens. Mot. Res.* *18*, 91–100.
- Shimegi, S., Ichikawa, T., Akasaki, T., and Sato, H. (1999). Temporal characteristics of response integration evoked by multiple whisker stimulations in the barrel cortex of rats. *J. Neurosci.* *19*, 10164–10175.
- Shimozawa, T., and Kanou, M. (1984). Varieties of filiform hairs: range fractionation by sensory afferents and cercal interneurons of a cricket. *J. Comp. Physiol.* *155*, 485–493.
- Shoykhet, M., Doherty, D., and Simons, D.J. (2000). Coding of deflection velocity and amplitude by whisker primary afferent neurons: implications for higher level processing. *Somatosens. Mot. Res.* *17*, 171–180.
- Simons, D.J. (1985). Temporal and spatial integration in the rat SI vibrissa cortex. *J. Neurophysiol.* *54*, 615–635.
- Simons, D.J., and Carvell, G.E. (1989). Thalamocortical response transformation in the rat vibrissa/barrel system. *J. Neurophysiol.* *61*, 311–330.
- Swadlow, H.A. (2003). Fast-spike interneurons and feedforward inhibition in awake sensory neocortex. *Cereb. Cortex* *13*, 25–32.
- van Netten, S.M., and Khanna, S.M. (1993). Mechanical demodulation of hydrodynamic stimuli performed by the lateral line organ. *Prog. Brain Res.* *97*, 45–51.
- von Békésy, G. (1947). The variation of phase along the basilar membrane with sinusoidal vibrations. *J. Acoust. Soc. Am.* *19*, 452–460.
- Woolsey, T.A., and Van der Loos, H. (1970). The structural organization of layer IV in the somatosensory region (SI) of mouse cerebral cortex. The description of a cortical field composed of discrete cytoarchitectonic units. *Brain Res.* *17*, 205–242.
- Yohro, T. (1977). Structure of the sinus hair follicle in the big-clawed shrew, *Sorex unguiculatus*. *J. Morphol.* *153*, 333–353.
- Zhu, J.J., and Connors, B.W. (1999). Intrinsic firing patterns and whisker-evoked synaptic responses of neurons in the rat barrel cortex. *J. Neurophysiol.* *81*, 1171–1183.
- Zucker, E., and Welker, W.I. (1969). Coding of somatic sensory input by vibrissae neurons in the rat's trigeminal ganglion. *Brain Res.* *12*, 138–156.